

Temperature dependent Al-induced crystallization of amorphous Ge thin films on SiO₂ substrates

著者別名	都甲 薫, 末益 崇
journal or publication title	Journal of crystal growth
volume	372
page range	189-192
year	2013-06
権利	(C) 2013 Elsevier B.V. NOTICE: this is the author's version of a work that was accepted for publication in Journal of crystal growth. Changes resulting from the publishing process, such as peer review, editing, corrections, structural formatting, and other quality control mechanisms may not be reflected in this document. Changes may have been made to this work since it was submitted for publication. A definitive version was subsequently published in Journal of crystal growth, Volume 372, 2013, DOI:10.1016/j.jcrysgr.2013.03.031
URL	http://hdl.handle.net/2241/119443

doi: 10.1016/j.jcrysgr.2013.03.031

1 **Temperature dependent Al-induced crystallization of amorphous Ge thin films on SiO₂**
2 **substrates**

3
4 Kaoru Toko^a, Naoki Fukata^b, Koki Nakazawa^a, Masashi Kurosawa^c, Noritaka Usami^d,
5 Masanobu Miyao^c, and Takashi Suemasu^a

6
7 ^a *Institute of Applied Physics, University of Tsukuba, Tsukuba, Ibaraki 305-8573, Japan*

8 ^b *National Institute for Materials Science, Namiki, Tsukuba, 305-0044, Japan*

9 ^c *Department of Electronics, Kyushu University, Motoooka, Fukuoka 819-0395, Japan*

10 ^d *Institute of Materials Research, Tohoku University, Sendai, Miyagi 980-8577, Japan*

11

12

13

14

15

16

17 *Keywords:* A1.Crystal orientation, A2.Solid phase crystallization, B1.Polycrystalline films;

18 B2.Semiconducting germanium

19

20 High-quality crystalline Ge thin-films on low-cost glass substrates are desired to reduce the
21 fabrication cost of high-efficiency tandem solar cells. We applied an Al-induced
22 crystallization technique to amorphous-Ge films (50-nm thickness) on SiO₂ glass substrates.
23 The annealing temperature of the sample strongly influenced the grain size and the crystal
24 orientation in the grown polycrystalline Ge layers: low annealing temperatures resulted in
25 large grains and high (111)-orientation fractions. As a result, annealing at 325 °C provided
26 98% (111)-oriented grains with average diameters of 30-μm. Moreover, the grown Ge layers
27 could be used as an epitaxial template for chemical vapor deposition. This large-grained Ge
28 film on a SiO₂ substrate appears promising for use as a Ge light-absorbing layer, as well as an
29 epitaxial buffer layer for group III-V compound semiconductors.

30

31 **1. Introduction**

32 Germanium has been used in the bottom cell of high-efficiency tandem solar cells
33 because of its desirable characteristics, such as its narrow band gap (0.66 eV), large
34 absorption coefficient ($\sim 10^4 \text{ cm}^{-1}$ at 1.1 eV), and good lattice matching to group III-V
35 compound semiconductors (0.1% lattice mismatch with GaAs) [1]. However, bulk Ge
36 substrates are extremely expensive, which has limited their application to special uses, such as
37 in tandem solar cells for space satellites. One promising approach to reducing fabrication cost
38 is substituting the bulk Ge substrate with a high-quality Ge thin film on a low-cost glass
39 substrate. Here, a low-temperature process ($< 550 \text{ }^\circ\text{C}$) is required to avoid softening the glass
40 substrate. Considering the absorption coefficient of Ge, the optimum thickness of the Ge layer
41 is calculated to be approximately 3- μm . In order to be able to draw photoexcited carriers to
42 the bottom and top electrodes, the grain size in the Ge layer should be larger than 3- μm in
43 diameter, because grain boundary scattering quenches the photoexcited carriers. Specifically,
44 a polycrystalline Ge (poly-Ge) layer works almost as well as a single-crystal Ge substrate if
45 the grain size is sufficiently large and the crystallinity of each grain is sufficiently high. A
46 promising technique for forming large-grained group III-V compound semiconductors for the
47 middle or top cells is epitaxial growth from each grain of the bottom Ge layer [2]. Regarding
48 the crystal orientation, (111)-oriented Ge is favorable for forming nanowires, which
49 dramatically enlarge the light-absorbing area [3, 4]. Many researchers have developed

50 advanced growth techniques: solid-phase crystallization (SPC) [5-7], metal-induced SPC
51 [8-10], laser annealing [11-13], and chemical vapor deposition (CVD) [14]. However, the
52 resulting Ge layers consist of small, submicron grains, with nearly random orientations.

53 Aluminum-induced crystallization (AIC) is a metal-induced SPC technique developed
54 for amorphous-Si (a-Si) films on glass substrates [15-23]. CVD of Si layers onto the AIC-Si
55 thin film is a promising approach to fabricating low-defect, large-grained Si layers on glass
56 substrates [24, 25]. However, AIC of amorphous Ge (a-Ge) had been difficult to accomplish
57 [26-29]. Recently, we realized Ge-AIC by preparing thin Ge and Al layers (50-nm thickness)
58 and optimizing the thickness of the AlO_x interfacial layer (~ 1 nm) [30]. This resulted in
59 preferentially (111)-oriented ($\sim 68\%$) poly-Ge films with relatively large-grains (5- μm
60 diameters). In this paper, the (111)-orientation fraction and the grain size are dramatically
61 improved by lowering the annealing temperature. Moreover, we demonstrate the usability of
62 the Al-induced crystallized Ge (AIC-Ge) films as an epitaxial template for large-grained
63 active Ge layers.

64

65 **2. Experimental procedure**

66 The preparation of the Al and Ge layers on quartz glass (SiO_2) substrates was carried
67 out at room temperature using a radio-frequency magnetron sputtering method. The
68 deposition times were 2.5 minutes for Al and 2.2 minutes for Ge, respectively. Between the

69 two deposition cycles, the Al films were exposed to air for 5 minutes to form native AlO_x
70 layers, in order to form a diffusion control layer. The thicknesses of the Al and a-Ge layers
71 were selected to be 50 nm each, because this thickness is favorable for the AIC growth of
72 a-Ge [30]. Finally, the samples were annealed at 325-400 °C in N_2 for 1-100 h. The surface
73 morphologies of the Ge layers were observed by Nomarski optical microscopy and scanning
74 electron microscopy (SEM). The Raman spectra were recorded using a Jobin Ivon Raman
75 microprobe system, with an Ar^+ laser (514.5 nm) excitation in a backscattering geometry.
76 θ - 2θ x-ray diffraction (XRD) measurements were performed using a Rigaku SmartLab system
77 with a Ge monochromator at a wavelength of 1.54 Å. The grain size and crystal orientation
78 were evaluated by electron backscattered diffraction (EBSD) measurement. Prior to the EBSD
79 measurement, the aluminum and oxide layers on the Ge layers were etched using an HF
80 solution (HF: 1.5%) for one minute.

81

82 **3. Results and Discussion**

83 Figs. 1(a) shows the expected schematic diagrams of the respective crystallization
84 stages, that is, Ge diffusion into Al, Ge lateral growth, and layer exchange. Each diagram
85 corresponds to its respective Nomarski optical micrograph in Fig. 1(b). These micrographs
86 show the back surface of the sample observed through the transparent quartz substrate. The
87 annealing temperature is 375 °C. These micrographs suggest that the Ge atoms diffuse to the

88 back surface, grow laterally, and cover the entire substrate during the annealing. The Raman
89 spectra in Fig. 1(c) show the appearance of a large peak after annealing. This peak, at around
90 295 cm^{-1} , originates from the vibration mode of Ge-Ge bonds, indicating the crystallization of
91 the Ge layer through the layer exchange process. These results typically demonstrate the
92 completion of AIC of a-Ge on a quartz glass substrate.

93 The EBSD measurement statistically characterizes the crystal orientation of the AIC-Ge,
94 as a function of the annealing temperature ($400\text{ }^{\circ}\text{C}$, $375\text{ }^{\circ}\text{C}$, $350\text{ }^{\circ}\text{C}$, and $325\text{ }^{\circ}\text{C}$). The
95 lower the annealing temperature, the longer the annealing time required for completion of the
96 AIC: (a) 1 h ($400\text{ }^{\circ}\text{C}$), (b) 10 h ($375\text{ }^{\circ}\text{C}$), (c) 30 h ($350\text{ }^{\circ}\text{C}$), and (d) 100 h ($325\text{ }^{\circ}\text{C}$). The
97 crystal orientation maps along the normal (z) and in-plane (x) directions relative to the sample
98 surfaces are respectively shown in Figs. 2(a)-2(d) and Figs. 2(e)-2(h). We can estimate the
99 grain size from the in-plane orientation maps, because the in-plane crystal directions are
100 different among the respective grains. The orientation maps in Fig. 2 clearly indicate that the
101 orientation and grain size of the AIC-Ge layers strongly depend on the annealing temperature:
102 a lower annealing temperature results in a dominant (111) orientation and a larger grain size in
103 the AIC-Ge layers.

104 The EBSD analysis is used to derive the area-fractions of the (111) orientation; the
105 average grain size from the EBSD maps is shown in Figs. 2(a)-2(h). The result is shown in
106 Fig. 3(a). By definition, the (111) fraction contains planes with tilt that is within 10° of the

107 exact (111) plane. Fig. 3(a) clearly indicates that both the (111) fraction and the grain size
108 increase with decreasing annealing temperature. As a result, the (111) fraction is as high as
109 98% and the grain size is as large as 30- μm diameter for an annealing temperature of 325 $^{\circ}\text{C}$.
110 These values are the highest among those previously reported for poly-Ge layers on
111 amorphous substrates in low-temperature processes [5-14]. In our previous work on AIC-Ge
112 annealed at 410 $^{\circ}\text{C}$ [30], the (111) fraction and the grain size were limited to 68% and 5 μm ,
113 respectively. Therefore, we can conclude that lowering the annealing temperature is very
114 important for enhancing the quality of the poly-Ge films in this AIC technique.

115 Next we discuss the annealing temperature dependence of the growth morphology. Ge
116 nucleation models are illustrated in Fig. 3(b). In the AIC of Si, it has been reported that Si
117 nucleation occurs when the Si concentration in the Al saturates at a level above the solubility
118 limit [15,17,19,20]. In particular, Sarikov *et al.* clarified that the supersaturation level of Al
119 with Si becomes higher when the annealing temperature is lowered [19]. This mechanism
120 should be the same for the AIC of Ge. During annealing, Ge atoms gradually diffuse into the
121 Al layer through the interfacial AlO_x layer. When the supersaturation level is low, the Ge
122 concentration saturates in the bulk Al before the Ge atoms reach the SiO_2 surface. Because Ge
123 nucleation occurs homogeneously in the bulk Al, the orientation becomes random as shown in
124 Fig. 3(b). In contrast, when the supersaturation level is high, Ge atoms can reach the SiO_2
125 surface without supersaturation occurring, and without homogeneous nucleation occurring in

126 the bulk Al. In the case of heterogeneous nucleation, the interfacial energy determines the
127 preferential orientation of the nuclei [19, 31]. Because the (111) plane has the lowest
128 interfacial energy in the diamond structure, (111)-oriented Ge nucleation occurs
129 heterogeneously on the SiO₂ surface [32]. Therefore, the preference for the (111) orientation
130 increases as the annealing temperature decreases. For the AIC technique, the initial nucleation
131 density determines the grain size because lateral growth stops when the growth fronts collide
132 [20]. Because a higher supersaturation level causes a lower nucleation rate [17,19], using a
133 low annealing temperature results in a large-grained poly-Ge film.

134 We investigated epitaxial thickening of Ge on the AIC-Ge (grown at 350 °C) using the
135 CVD technique to confirm that this AIC-Ge can be used as an epitaxial template for advanced
136 materials and nanowires. In the CVD, we employed a GeH₄ gas source and kept the sample
137 substrate at 450 °C. A 200-nm thick Ge layer was grown on the AIC-Ge film. The SEM and
138 EBSD images of the CVD-thickened sample surface are shown in Figs. 4(a) and 4(b),
139 respectively. The CVD layer clearly shows predominantly (111) orientation. This result
140 indicates CVD epitaxial growth of the Ge layer on the AIC-Ge film, because conventional
141 CVD-Ge layers without AIC-Ge templates consist of small grains with random orientations
142 [14].

143 XRD measurements are performed to evaluate the epitaxial relationship between the
144 CVD-Ge and AIC-Ge layers. Fig. 5(a) shows the XRD patterns taken from θ - 2θ

145 measurements for the samples before and after CVD thickening. In both patterns, sharp peaks
146 are observed at around 27° , which corresponds to the Ge (111) plane. This figure clearly
147 shows that the CVD thickening strongly enlarges the Ge (111) peak, and other peaks do not
148 appear. A reciprocal space map was obtained around the Ge (111) plane and is shown in Fig.
149 5(b). A wide contour is observed in the reciprocal space map, which reflects the tilted (111)
150 planes. The maximum tilt angle is calculated to be 12 degrees. This contour has only a single
151 peak, which suggests that the orientation of the AIC-Ge and CVD-Ge layers is the same, due
152 to homoepitaxial growth. The lattice constant of the Ge layer is calculated to be 5.658 \AA from
153 the peak position, a value that is almost the same as the relaxed Ge lattice constant (5.66 \AA).
154 Therefore, we have demonstrated the usability of this AIC-Ge thin film on an insulator as an
155 epitaxial template for the CVD-Ge layer. It is expected that epitaxial growth of other
156 advanced materials and unidirectionally aligned nanowires is possible using this technique.

157

158 **4. Conclusions**

159 We have investigated the Al-induced crystallization (AIC) of an a-Ge film (50-nm
160 thickness) on an insulator. The crystallization of the a-Ge layer occurred through the
161 layer-exchange process. We found that the annealing temperature of the sample strongly
162 influenced the grain size and crystal orientation in the grown Ge layers: a lower annealing
163 temperature yielded larger grains and a higher (111)-orientation fraction. Annealing at 325°C

164 increased the grain size to up to 30- μm in diameter and the (111)-orientation fraction to up to
165 98%. Moreover, the grown Ge layers proved suitable for use as an epitaxial template for
166 chemical vapor deposition (CVD). This large-grained Ge layer on an insulator holds promise
167 for use as a Ge light-absorbing layer and as an epitaxial buffer layer, not only for group III-V
168 compound semiconductors, but also for nanowires and other advanced materials.

169

170 **Acknowledgements**

171 This work was partially supported by a Grant-in-Aid for Scientific Research from the
172 Ministry of Education, Culture, Sport, Science, and Technology in Japan.

173

174 **References**

- 175 [1] R.R. King, D.C. Law, K.M. Edmondson, C.M. Fetzer, G.S. Kinsey, H. Yoon, R.A. Sherif,
176 N.H. Karam, Appl. Phys. Lett. **90** (2007) 183516.
- 177 [2] M.G. Mauk, J.R. Balliet, B.W. Feyock, J. Cryst. Growth **250** (2003) 50.
- 178 [3] N. Fukata, K. Sato, M. Mitome, Y. Bando, T. Sekiguchi, M. Kirkham, J. I. Hong, Z. L.
179 Wang, R. L. Snyder, ACS Nano **4** (2010) 3807.
- 180 [4] E.P. M. Bakkers, J. van Dam, S. De Franceschi, L.P. Kouwenhoven, M. Kaiser, M.
181 Verheijen, H. Wondergem, P. van der Sluis, Nature Materials **3** (2004) 769.
- 182 [5] C.Y. Tsao, J.W. Weber, P. Campbell, P.I. Widenborg, D. Song, M.A. Green, Appl. Surf. Sci.
183 **255** (2009) 7028.
- 184 [6] A.F. Khan, M. Mehmood, A.M. Rana, T. Muhammad, Appl. Surf. Sci. **256** (2010) 2031.
- 185 [7] K. Toko, I. Nakao, T. Sadoh, T. Noguchi, M. Miyao, Solid-State Electron. **53** (2009) 1159.
- 186 [8] H. Kanno, K. Toko, T. Sadoh, M. Miyao, Appl. Phys. Lett. **89** (2006) 182120.
- 187 [9] J.H. Park, P. Kapur, K.C. Saraswat, H. Peng, Appl. Phys. Lett. **91** (2007) 143107.
- 188 [10] K. Toko, H. Kanno, A. Kenjo, T. Sadoh, T. Asano, M. Miyao, Appl. Phys. Lett. **91** (2007)
189 042111.
- 190 [11] H. Watakabe, T. Sameshima, H. Kanno, M. Miyao, Thin Solid Films **508** (2006) 315.
- 191 [12] W. Yeh, H. Chen, H. Huang, C. Hsiao, J. Jeng, Appl. Phys. Lett. **93** (2008) 094103.
- 192 [13] K. Sakaike, S. Higashi, H. Murakami, S. Miyazaki, Thin Solid Films **516** (2008) 3595.

- 193 [14] M. Tada, J.H. Park, J.R. Jain, K.C. Saraswat, *J. Electrochem. Soc.* **156** (2009) D23.
- 194 [15] O. Nast, T. Puzzer, L.M. Koschier, A.B. Sproul, S.R. Wenham, *Appl. Phys. Lett.* **73**
195 (1998) 3214.
- 196 [16] Y. Sugimoto, N. Takata, T. Hirota, K. Ikeda, F. Yoshida, H. Nakashima, H. Nakashima,
197 *Jpn. J. Appl. Phys.* **44** (2005) 4770.
- 198 [17] J. Schneider, A. Sarikov, J. Klein, M. Muske, I. Sieber, T. Quinn, H.S. Reehal, S. Gall, W.
199 Fuhs, *J. Cryst. Growth* **287** (2006) 423.
- 200 [18] J.Y. Wang, Z.M. Wang, and E.J. Mittemeijer, *J. Appl. Phys.* **102** (2007) 113523.
- 201 [19] A. Sarikov, J. Schneider, J. Berghold, M. Muske, I. Sieber, S. Gall, W. Fuhs, *J. Appl.*
202 *Phys.* **107** (2010) 114318.
- 203 [20] B.I. Birajdar, T. Antesberger, B. Butz, M. Stutzmann, E. Spiecker, *Scripta Materialia* **66**
204 (2012) 550.
- 205 [21] M. Kurosawa, N. Kawabata, T. Sadoh, M. Miyao, *Appl. Phys. Lett.* **95** (2009) 132103.
- 206 [22] M. Jung, A. Okada, T. Saito, T. Suemasu, N. Usami, *Appl. Phys. Express* **3** (2010)
207 095803.
- 208 [23] M. Kurosawa, K. Toko, N. Kawabata, T. Sadoh, M. Miyao, *Solid-State Electron.* **60**
209 (2011) 7.
- 210 [24] I. Gordon, L. Carnel, D.V. Gestel, G. Beaucarne, J. Poortmans, *Thin Solid Films* **516**
211 (2008) 6984.

- 212 [25] B.R. Wu, S.Y. Lo, D.S. Wu, S.L. Ou, H.Y. Mao, J.H. Wang, R.H. Horng, *Thin Solid*
213 *Films* **520** (2012) 5860.
- 214 [26] F. Katsuki, K. Hanafusa, M. Yonemura, T. Koyama, M. Doi, *J. Appl. Phys.* **89** (2001)
215 4643.
- 216 [27] S. Hu, A.F. Marshall, P.C. McIntyre, *Appl. Phys. Lett.* **97** (2010) 082104.
- 217 [28] Z. Wang, J. Wang, L. Jeurgens, E. Mittemeijer, *Phys. Rev. B* **77** (2008) 1.
- 218 [29] S. Peng, D. Hu, D. He, *Appl. Surf. Sci.* **258** (2012) 6003.
- 219 [30] M. Kurosawa, N. Kawabata, T. Sadoh, M. Miyao, *ECS J. Solid State Sci. and Tech.* **1**
220 (2012) 144.
- 221 [31] C. Spinella, S. Lombardo, F. Priolo, *J. Appl. Phys.* **84** (1998) 5383.
- 222 [32] A.A. Stekolnikov, J. Furthmuller, F. Bechstedt, *Phys. Rev. B* **65** (2002) 115318.

223 **Fig. 1.** (a) Schematic structures of the expected growth stage during AIC of a-Ge. (b)
224 Nomarski optical micrographs of the back surface of the sample annealed at 375 °C for 0 h, 2
225 h, and 10 h. (c) Raman spectra before and after annealing. The peak at 295 cm⁻¹ corresponds
226 to the Ge-Ge vibration mode.

227

228 **Fig. 2.** EBSD images of the AIC-Ge surfaces after annealing at 400 °C, 375 °C, 350 °C,
229 and 325 °C. (a)-(d) normal (z) and (e)-(h) in-plane (x) directions with respect to the sample
230 surface. The colors indicate the crystal orientation, according to the inserted color keys.

231

232 **Fig. 3.** (a) The (111)-orientation area-fraction and grain size of the AIC-Ge layers as a
233 function of the annealing time. (b) Schematic model of the temperature-dependent
234 (111)-orientation fraction and grain size: (111)-oriented nuclei are generated at the Ge/SiO₂
235 interface.

236

237 **Fig. 4.** (a) SEM and (b) EBSD images of the thickened Ge layer grown on the AIC-Ge
238 template.

239

240 **Fig. 5.** XRD characterization of the thickened Ge layer grown on the AIC-Ge template. (a)
241 XRD patterns obtained by θ - 2θ measurements before and after CVD-thickening and (b)

242 reciprocal space mapping taken around the Ge (111) reflection.

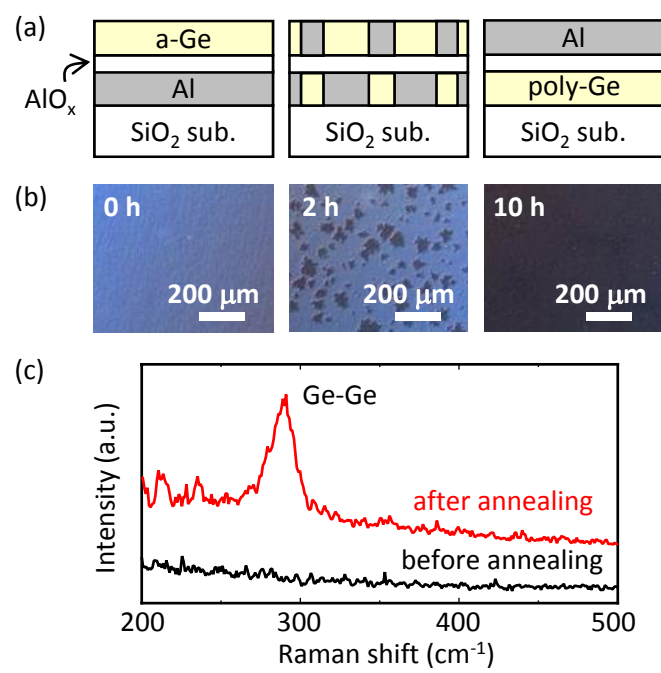


Figure 1 K. Toko

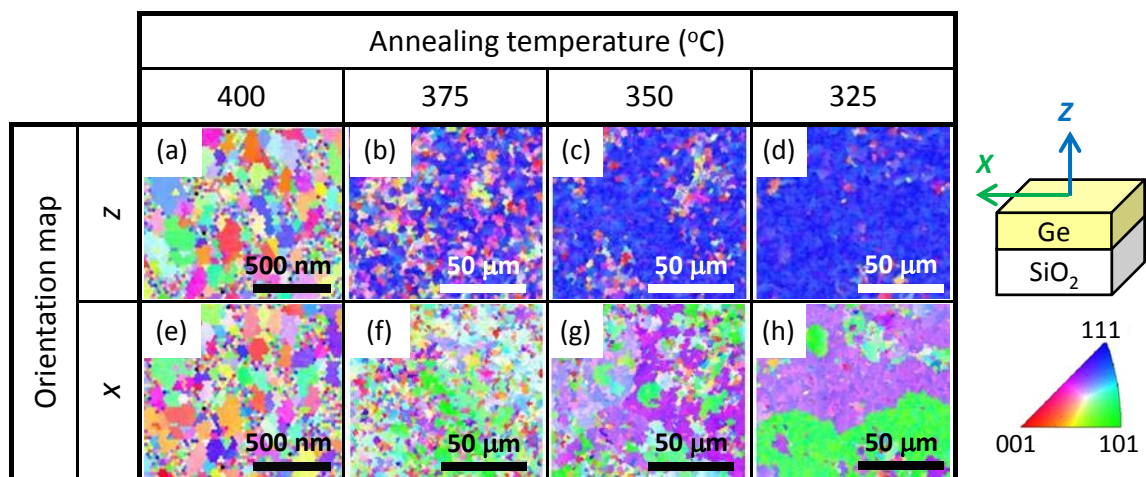


Figure 2 K. Toko

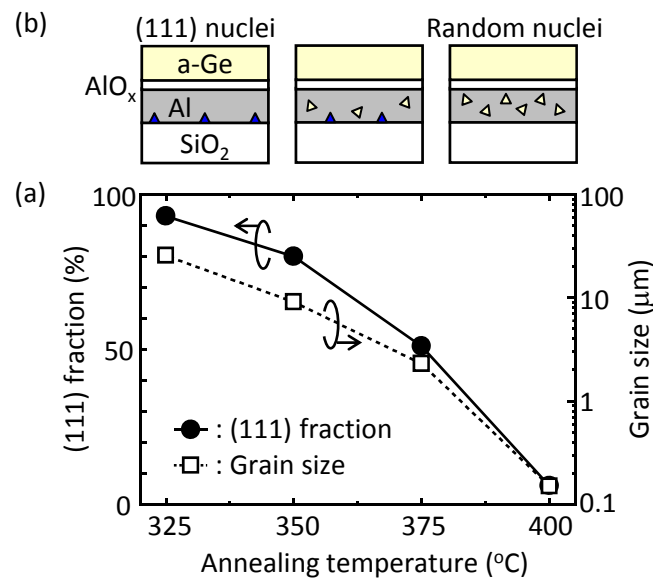
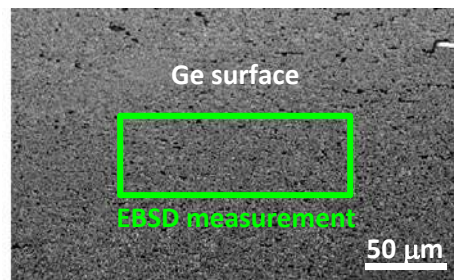


Figure 3 K. Toko

(a)



(b)

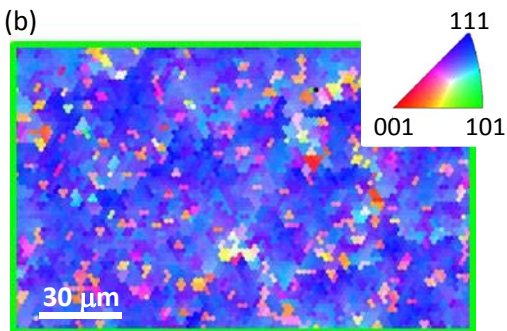


Figure 4 K. Toko

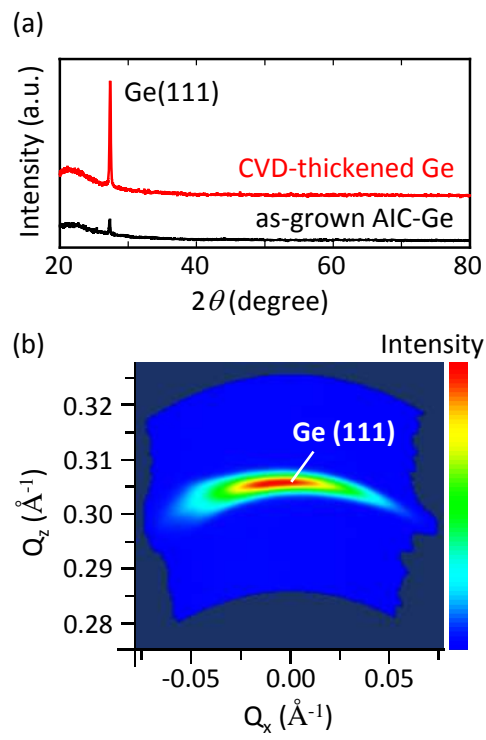


Figure 5 K. Toko